Radiative relaxation in isolated large carbon clusters: Vibrational emission versus recurrent fluorescence

Ozan Lacinbala, Florent Calvo, Clément Dubosq, C. Falvo, Pascal Parneix, Mathias Rapacioli, Aude Simon, Thomas Pino

▶ **To cite this version:**

Ozan Lacinbala, Florent Calvo, Clément Dubosq, C. Falvo, Pascal Parneix, et al.. Radiative relaxation in isolated large carbon clusters: Vibrational emission versus recurrent fluorescence. Journal of Chemical Physics, 2022, 156 (4), pp.144305. 10.1063/5.0080494 . hal-03689196

HAL Id: hal-03689196
https://hal.science/hal-03689196

Submitted on 12 Oct 2022

HAL is a multi-disciplinary open access archive for the deposit and dissemination of scientific research documents, whether they are published or not. The documents may come from teaching and research institutions in France or abroad, or from public or private research centers.

L'archive ouverte pluridisciplinaire **HAL**, est destinée au dépôt et à la diffusion de documents scientifiques de niveau recherche, publiés ou non, émanant des établissements d'enseignement et de recherche français ou étrangers, des laboratoires publics ou privés.

Radiative relaxation in isolated large carbon clusters: vibrational emission versus recurrent fluorescence

O. Lacinbala,[1] F. Calvo,[2] C. Dubosq,[3] C. Falvo,[1,2] P. Parneix,[1] M. Rapacioli,[3] A. Simon,[3] and T. Pino[1]
[1)] *Université Paris-Saclay, CNRS, Institut des Sciences Moléculaires d'Orsay (ISMO), 91405 Orsay, France*
[2)] *Université Grenoble-Alpes, CNRS, LIPhy, 38000, Grenoble*
[3)] *Laboratoire de Chimie et Physique Quantiques (LCPQ), Fédération FeRMI, Université de Toulouse, CNRS, 31062, Toulouse*

(*Electronic mail: thomas.pino@universite-paris-saclay.fr)

(*Electronic mail: ozan.lacinbala@universite-paris-saclay.fr)

(Dated: 12 October 2022)

Recurrent fluorescence (RF) from isolated carbon clusters containing between 24 and 60 atoms is theoretically investigated as a function of internal energy, cluster size and structural features. The vibrational relaxation kinetics and the associated IR emission spectra are determined by means of a Monte Carlo approach with vibrational densities of states computed in the harmonic approximation. RF is generally found to be highly competitive with vibrational emission. The behaviors predicted for clusters of various sizes and archetypal structures indicate that the IR emission spectra are strongly influenced by RF, an energy gap law being obtained for the evolution of the RF rate constant depending on the electronic excitation state. The present results are relevant to the photophysics of the interstellar medium and could contribute to elucidating the carriers of the extended red emission bands as well as the continuum emission lying below the aromatic infrared bands believed to originate from mixed aromatic-aliphatic compounds.

I. INTRODUCTION

The sp, sp^2 and sp^3 hybridizations exhibited by carbon are a central component of organic chemistry and explain the various allotropic forms of carbon, including its different crystalline phases of diamond, lonsdaleite and graphite, as well as the amorphous phase. At the nanoscale, structural diversity is manifested by the existence of a great variety of carbon clusters, but also nanotubes and graphene itself.[1–4] In particular, the detailed structures of pure carbon cluster ions have been investigated and detected for C_{24}, C_{40}, C_{60} and even larger clusters using ion mobility experiments.[5–10] It has been established from these experiments that cages, graphitic and ring isomers of carbon clusters are sufficient stable to be detected. Recently, motivated by astrophysical issues, the structural diversity of carbon clusters was also explored from the perspective of their infrared and electronic spectra.[4,11,12] A systematic exploration of the structures themselves,[4] carried out by means of molecular simulation and a systematic sampling based on the REBO reactive potential,[13] revealed that in the range between 24 and 60 atoms, carbon clusters can be classified into four main families depending essentially on their aromatic content and overall shape: cages, that include fullerenes; flakes, that can be defined as mostly planar polycyclic aromatic compounds; pretzel-like structures,[14] with a more open character and long carbon chains; and finally branched structures with terminating sp carbons. From a knowledge of these structures, both the vibrational[11] and optical[12] spectra were subsequently determined using an efficient electronic structure method, namely self-consistent charge density-functional based tight-binding (SCC-DFTB)[15] and its time dependent version.[16]

Carbon clusters are found notably as products of incomplete combustion,[17–19] and several of them have been detected in the interstellar medium (ISM). Owing to combined efforts from observation, experiments and simulations, it is now known that a large fraction of carbon in Space is included in large carbonaceous molecules and dust grains. The former could be (nano-)diamonds, fullerenes, polycyclic aromatic structures, amorphous carbon and their hydrogenated amorphous carbon forms.[20] In particular, C_{60} buckminsterfullerene and C_{70} have been identified through their infrared emission spectra in several ISM environments (reflection nebulae, planetary nebulae, protoplanetary nebulae, diffuse medium)[21–26] and the C_{70} in Tc 1 planetary nebulae.[22] The C_{60} buckminsterfullerene cation has also been detected in absorption,[27] likely in emission too[28] and five diffuse interstellar bands have been attributed to it.[29–31] Interestingly, smaller clusters such as C_2 (Ref. 32) C_3 (Ref. 33) or C_5 (Ref. 34) have also been detected.

From the point of view of interstellar absorption spectroscopy, carbon clusters with a high aromatic content such as fullerenes or flakes may contribute to the UV-bump at 217.5 nm.[12] Two main models have been proposed to explain the presence of fullerenes in the ISM. In the so-called top-down model, large polycyclic aromatic hydrocarbons (PAHs) experience UV irradiation and consequently undergo dehydrogenation, fragmentation and then isomerization to form pentagon rings until they reach a cage shape.[35,36] In the alternative bottom-up scenario, the growth of fullerenes is explained by the successive incorporation of individual carbon atoms or dimers, a mechanism known as closed network growth.[37]

Owing to their reasonably large size and great structural diversity, these clusters can exhibit low lying electronic excited states in the vicinity of vibrational excited states. This proximity makes the photophysics of carbon clusters particularly interesting. In the present work, we further exploit the large database of structures made available from previous studies in

the context of photophysical evolution,[4,11,12] and address their relaxation kinetics upon absorption of a UV photon.

Upon excitation, which may be electronic or vibrational, a large molecule can undergo various relaxation processes acting on the different degrees of freedom and operating over different time scales, and which include electronic fluorescence, internal conversion or intersystem crossing, isomerization, ionization or fragmentation. One typical situation is that of internal conversion or intersystem crossing, in which the initial electronic energy is entirely converted into nuclear motion, leading the system into the electronic ground state but with a high vibrational energy. Relaxation proceeds subsequently through emission of IR photons (vibrational emission),[38,39] in competition with fragmentation and isomerization if these pathways are open at the available internal energy. In the case of carbon cluster ions, radiative cooling has been specifically investigated in the size range of 36–96 atoms,[40–45] in smaller carbon clusters[46–51] and perylene cation as well,[52] especially by means of electrostatic storage rings.

However, it is also possible that a part of the vibrational energy flows back into the electronic degrees of freedom, especially if there are some low-lying electronic excited states as in the case of carbon clusters. In this process called inverse internal conversion, the internal energy is sufficient to possibly induce spontaneous electronic excitation, after which the molecule can again relax through electronic fluorescence or non-radiative processes. When electronic fluorescence occurs after such inverse internal conversion, it is usually referred to as recurrent or Poincaré fluorescence.[53]

In the context of photophysics in the ISM, recurrent fluorescence (RF) has been suggested as a likely relaxation pathway for PAH emission[53], and RF of large carbon clusters is suspected to be a possible cause for the extended red emission detected in several interstellar environments (reflection nebulae, HII regions, carbon-rich planetary nebulae, diffuse interstellar medium, galactic cirrus clouds and in other galaxies) and particularly in the Red Rectangle.[54–56] RF is also suspected to contribute to the continuum of the near-IR emission[57]. In very hot environments such as flames, carbon clusters are so highly vibrationally excited that RF may extend over the near-IR and visible wavelength ranges.[58,59] Recently, evidence for RF taking place in (hydro)carbon clusters such as PAH cations, anthracene,[60] naphthalene,[61] small carbon clusters C_n^+, $n = 8, 10, 13-16$ (Ref. 49), the C_6^- anion,[62,63] as well as metallic Co_n^+ (n=5–23) clusters[64] was provided in experiments in which the relaxation could be monitored over long times in electrostatic storage rings. RF can be fairly suspected to occur in neutral species as well, even though, to our best knowledge, it remains to be observed.

The purpose of the present work is to obtain more insight into the possible competition between recurrent fluorescence and vibrational emission occurring in isolated large carbon clusters and the dependence of both processes on the internal energy, the size and the structural features of these clusters. We have chosen to focus on archetypal isomers of C_{60} that belong to the four structural families identified in our earlier contribution,[4] and to selected structures of the smaller C_{42} and C_{24} clusters, both taken from the sample of flake isomers.

To quantify the relative efficiencies of recurrent fluorescence and vibrational emission, we employ a kinetic Monte Carlo model that uses static vibrational and electronic data obtained from electronic structure calculations and assumes an harmonic approximation for the level densities. Using appropriate expressions for the various rate constants associated to the different relaxation pathways, the time evolution of the internal energy of the system can be monitored and the radiative cooling mechanisms can be addressed in detail.

The article is organized as follows. The theoretical and computational details of our approach are detailed in Sec. II, while Sec. III is devoted to its application to several isolated carbon clusters of selected size and shape. In Sec. IV we discuss the dependence of the RF rate on the electronic state energy and find some connection with the energy gap law[65,66] in the context of radiationless transitions. We also elaborate further on the relation between RF efficiency and structural features, extending much beyond our reduced selection of archetypal isomers, by considering now a thousand of them. Finally, Sec. V summarizes the main findings of our work and draws some conclusions and perspectives.

II. METHODS

Before laying out the general theoretical framework, it is useful to recall the typical time scales associated with the various elementary radiative processes taking place in carbon clusters. Upon an electronic excitation, large molecules such as carbon clusters or carbonaceous aromatic compounds undergo internal conversion over $\sim 10^{-14}$–10^{-8} s. Intersystem crossing occurs over $\sim 10^{-10}$–10^{-7} s, usually involving neighboring electronic states, until the electronic ground state is reached citebirks1970aromatic with the excess energy being converted mainly into vibrational motion. Concomitantly, intramolecular vibrational redistribution (IVR) typically proceeds over $\sim 10^{-13}$–10^{-10} s,[67,68] the vibrational energy being thus redistributed among all vibrational states so that the system reaches statistical equilibrium.

In contrast, the typical time scales for vibrational emission (VE) and recurrent fluorescence are $\sim 10^{-2}$–10^{1} s and $\sim 10^{-4}$–10^{1} s, respectively, much slower than internal conversion, intersystem crossing and IVR. We will thus safely assume as a statistical hypothesis that the vibrational energy in the ground electronic state is ergodically distributed between two successive emissions. In doing so, we neglect the contribution of rotational degrees of freedom to the total system energy.[69] However, for the present relatively large clusters, the rotational energy is negligible compared to the vibrational contribution, so we ignore it in our modeling. Various relaxation channels are a priori in competition for carbon clusters. These include radiative pathways, which are RF and VE as mentioned above, but also direct electronic fluorescence and non radiative relaxation channels such as dissociation and ionization.[70]

Our aim is to compute the emission spectra originating from the various radiative relaxation channels and their dynamical features. Here we follow a methodology already laid out in earlier contributions,[71,72] which relies on an event-driven ki-

netic Monte Carlo (kMC) approach where all possible relaxation events are enumerated for a given state of the system, the next state being stochastically advanced from the knowledge of the corresponding rate constants. The kMC simulation requires evaluating the entire set of rate constants associated with the various relaxation mechanisms, at the current internal state of the system. kMC is intrinsically microcanonical, as we do not consider the additional interaction between the system and the environment once the initial excitation has driven it out of equilibrium.

The emission spectrum is obtained from the accumulation of photons emitted over many independent realizations of the simulations, for a fixed observation time or until the system has reached its ground state or, in practice, a very low internal energy sufficient to make it stable over extremely long times.

A. Vibrational emission and recurrent fluorescence rate constants

We first discuss the case of vibrational emission, starting with the decay of vibrational energy on the ground electronic state by successive emission of IR photons.

In the harmonic approximation, the vibrational state of the system can be described from the knowledge of its vibrational frequencies $\{\omega_i, i = 1, \cdots, g\}$ where g denotes the number of vibrational modes. For a given internal energy E, the microcanonical probability $P_{i,v}$ that a specific mode i is occupied by v vibrational quanta reads

$$P_{i,v}(E) = \frac{\rho_{/i}(E - v\hbar\omega_i)}{\rho(E)}, \tag{1}$$

where $\rho(E)$ is the total ground state vibrational density of states at the internal energy E, $\rho_{/i}(E - v\hbar\omega_i)$ is the ground state vibrational density of states at the internal energy $E - v\hbar\omega_i$ without taking into account the i^{th} vibrational mode. This is made possible because we use the harmonic approximation for the vibrational density of states. From this probability, the emission rate constant from the i^{th} mode occupied by all possible v vibrational quanta is obtained as

$$A_i(E) = \sum_{v=1}^{v_{\max}} \frac{\rho_{/i}(E - v\hbar\omega_i)}{\rho(E)} A_i^{v\to v-1}, \tag{2}$$

where $A_i^{v\to v-1}$ is the one-photon emission rate from v upper level to the next lower level $v-1$ from the i^{th} mode, and $v_{\max}$ the maximum number of quanta that this mode can sustain at the current total energy, given by the integer part of $E/\hbar\omega_i$. Note that the total emission rate constant $A_i(E)$ is a weighted sum of all possible rate constants $A_i^{v\to v-1}$, individual weights being related to the occupation of the respective vibrational levels. In addition, we do not take into account overtones or combination bands, which we assume to be negligible compared to the direct $v \to v-1$ emissions. For harmonic oscillators we can further use the relation $A_i^{v\to v-1} = vA_i^{1\to 0}$, where $A_i^{1\to 0}$ is the Einstein coefficient of the fundamental transition of mode i. This allows the emission rate constant from the i^{th} vibrational mode to be rewritten as[73,74]

$$A_i(E) = A_i^{1\to 0} \sum_{v=1}^{v_{\max}} \frac{\rho_{/i}(E - v\hbar\omega_i)}{\rho(E)} \times v. \tag{3}$$

The emission rate constant $A_i(E)$ can be viewed as resulting from two different contributions, namely a quantum contribution through the Einstein coefficient $A_i^{1\to 0}$, and a statistical contribution which expresses the occupation of the vibrational levels and gives rise to a dependency of the emission rate on the internal energy. The Einstein coefficients are directly related to the frequency ω_i and the vibrational oscillator strength f_i of the mode through[75]

$$A_i^{1\to 0} = \frac{8\pi^3 e^2 \omega_i^2}{\varepsilon_0 m_e c^3} \times f_i. \tag{4}$$

Turning now to recurrent fluorescence, we again assume that owing to the much faster time for vibrational redistribution, the distribution of vibronic states is entirely statistical, not only in the ground electronic state but also for all accessible electronic excited states. The occupation probability of any n^{th} electronic state lying at energy E_n is proportional to $\rho_n(E - E_n)$, where $\rho_n(E - E_n)$ is the density of vibrational states on the corresponding electronic state at energy E_n relative to the ground electronic state. It should also be stressed here that the internal energy E is defined as the sum of the vibrational and electronic energies, relative to the ground electronic state at the minimum energy configuration.

Here we introduce two additional approximations. First, we assume that for relatively large systems as those under scrutiny in the present work, the vibrational structure is similar between the low-lying electronic states and the ground state, allowing us to write $\rho_n(E - E_n) \approx \rho_0(E - E_n)$. To simplify notations, the subscript 0 is removed from the vibrational density of states $\rho_0(E) = \rho(E)$, thus assumed not to depend on the electronic level. The probability of the n^{th} electronic state at thermal equilibrium thus reads

$$\gamma_n = \frac{\rho(E - E_n)}{\sum_k \rho(E - E_k)}, \tag{5}$$

where the denominator is a normalizing factor. In addition, the densities of states grow very fast with increasing energy, hence we approximate the sum in this denominator as its first, dominant term:

$$\gamma_n \simeq \frac{\rho(E - E_n)}{\rho(E)}. \tag{6}$$

This approximation is discussed and justified in more details in the Supplemental Information material, see Fig. S1.

The RF rate constant, which can be considered as an effective electronic fluorescence rate constant, is then written as

$$A_{\text{RF}}^{n\to 0}(E) = A_{\text{f}}^{n0} \frac{\rho(E - E_n)}{\rho(E)}. \tag{7}$$

For this process too the rate constant contains one quantum contribution in the prefactor, and a statistical contribution involving the densities of vibronic states. Moreover, the electronic fluorescence rate constant A_f^{n0} is expressed from Eq. (4)

in which f_i is the electronic oscillator strength and $\hbar\omega_i$ the electronic energy of the i^{th} excited electronic state.

For the sake of computational simplicity, we further neglect fluorescence between different electronic excited states and assume that only the $n \to 0$ transitions are efficient. Vibrational emission from electronically excited states can also be accounted for, using a similar expression as Eq. (3) above for the ground state but involving now the correctly shifted densities of states (still assuming $\rho_n \approx \rho_0 = \rho$):

$$A_i^n(E) = \frac{\rho(E-E_n)}{\rho(E)} A_i(E-E_n). \tag{8}$$

VE from electronically excited states is usually negligible compared to VE from the ground electronic states and to RF. Expressions (3), (7) and (8) are implemented for the simulation.

B. Approximate analytical expressions for the rate constants

For both RF and VE mechanisms, simple expressions can be obtained for the corresponding rate constants by considering specific approximations and limiting forms. The total rate constant for RF processes and its dependence on internal energy can be determined at high internal energy using a semiclassical expression for the harmonic vibrational density of states[76]

$$\rho(E) \approx \frac{(E+E_z)^{g-1}}{(g-1)!\prod_{i=1}^{g}\hbar\omega_i}, \tag{9}$$

where E is the internal energy and E_z the zero-point energy. Incorporating the latter expression inside Eq. (7) and assuming that $E + E_z \gg E_n$, the total RF rate constant can be expressed as

$$A_{\text{rec}}^{\text{tot}}(E) = \sum_{n=1}^{n_{\max}} A_f^{n0} \times \exp\left(-\frac{(g-1)E_n}{E+E_z}\right), \tag{10}$$

in which $n_{\max}$ is the highest electronic quantum number that is accessible at the internal energy E. Likewise, an analytical approximation can be obtained for the VE rate constant from the i^{th} vibrational mode using a continuous approximation for the discrete sum of Eq. (3). This approximation is also valid at high internal energies $E/\hbar\omega_i = v_{\max} \gg 1$ and yields:

$$A_i(E) \simeq A_i^{1\to 0}(g-1)\int_0^{v_{\max}} \mathrm{d}v\, \frac{v}{v_{\max}}\left(1-\frac{v}{v_{\max}}\right)^{g-2} \tag{11}$$

This integral can be solved exactly as

$$A_i(E) = A_i^{1\to 0}\frac{E}{g\hbar\omega_i} \tag{12}$$

in which we further neglected the zero-point contribution to the internal energy E, assumed to be high.

Summing over all VE rate constants eventually leads to

$$A_{\text{vib}}^{\text{tot}}(E) = \frac{E}{g}\sum_{i=0}^{n_{\max}} \frac{A_i^{1\to 0}}{\hbar\omega_i}. \tag{13}$$

Equations (9), (10) and (12) will be used for interpreting simulation results.

C. Other processes: C_2 or C_3 dissociation, delayed ionization and isomerization

When modeling the long-time relaxation decay of carbon clusters it is important to also consider the possible contribution of other non-radiative pathways. At high energies, thermal dissociation or fragmentation could be activated, and we have evaluated the propensity for such events through the traditional unimolecular reaction theories based on the Rice-Ramsperger-Kassel (RRK) framework.[76] More precisely, the dissociation rate constant can be expressed within this approach simply as

$$k_{\text{diss}}(E) = A(1-D/E)^{g-1}, \tag{14}$$

where D is the dissociation energy and A is a prefactor. For C_{60}, accepted values for $A = 10^{20}$ s^{-1} and $D = 10$ eV[77–81] yield a dissociation rate constant of 10^{-38} s^{-1} at the excess energy of 18.5 eV, which is the maximum value considered in the present work. For C_{42}, a similar prefactor and a dissociation energy of 7.5 eV[78,79,82] lead to a much higher dissociation rate constant of about 10^{-7} s^{-1}, although, and as seen below, still much slower than the processes we are focusing on.

To the best of our knowledge, no such data are available for C_{24}. The dissociation rate constant for this cluster can be estimated at 12.5 eV excess energy if we assume a prefactor $A = 3\cdot 10^{20}$ **s**$^{-1}$ and a conservative dissociation energy D of 6 eV only.[82,83] Such values lead to a dissociation rate constant of 35 **s**$^{-1}$. For this cluster, the neglect of thermal dissociation could be a more stringent approximation than for the two larger systems, for which dissociation is unlikely to occur at all under the conditions of our modeling.

However, in all cases we note that the actual dissociation process is a highly complex function of the isomer too, which further involves strong anharmonicities, making the rate constant determination quite difficult. Additionally, the RRK modeling used here for crude evaluation of the rate constants ignores the possibility of fragmentation on electronic excited states, which for carbon clusters was shown to be also a realistic pathway.[84]

Similarly, we also rule out the possibility of delayed (thermo)ionization, which is negligible for C_{60} compared to radiative emission by several orders of magnitude at the internal energies considered in this work.[70,77] Despite being of smaller size, the ionization threshold of the C_{24} and C_{42} clusters is higher than that of C_{60}.[70] We then further assume that delayed ionization will also be negligible for these clusters. On a side note, stimulated emission processes are altogether ignored since the systems under scrutiny are all isolated and remains so once they have been initially excited.

Another relaxation mode is that of isomerization, which could be recently experimentally evidenced on the small C_{10}^- cluster ion.[85] Accounting for isomerization processes on the same footing as electronic or vibrational relaxation for each individual isomer is in principle possible but would require, at least, the independent identification of transition states between connected isomers together with the evaluation of isomerization rate constants, e.g. from harmonic transition state theory. While such approaches have been used in the past to address the influence of kinetic rearrangement on spectroscopic properties,[86] they ignore the possibly important role of electronic excitation on which we focus here. Moreover we arbitrarily assume the multiple isomers of our samples to be uniformly distributed, treating their individual contribution in a statistical way. It should be noted that in our previous study,[4] temperatures well above 3500 K had to be used to realize efficient sampling of the potential energy surfaces in the REMD (Replica Exchange Molecular Dynamics) simulations. This is consistent with the result from[14] in which they found a melting temperature for 4000 K for C60 associated with a large structural reorganization. Isomerization in the considered energy range ($<$ 18.5 eV internal energy) is thus expected to be inefficient or only between rather similar isomer. In our phenomenological model, we thus choose to ignore individual isomerization.

D. Kinetic Monte Carlo modeling of emission cascades

We now incorporate the previously determined rates for vibrational and recurrent relaxations into an integrated framework in which the evolution of the system and its internal energy can be monitored as a function of time. The main idea is to enumerate all possible events for a given internal energy and calculate their absolute rate constants, then select one of them randomly based on a probability proportional to its rate constant.

In practice, owing to complete IVR between successive events, memory loss allows us to assume a Markovian process for the kMC procedure, and a time duration for the current state that follows Poissonian statistics.[87] From the knowledge of all individual rate constants, their sum Γ is determined and the duration δt of the current state is taken as $\delta t = -\log(\mathtt{ran})/\Gamma$, where ran is a uniform random number in the range $0 < \mathtt{ran} \leq 1$. Alternatively, a simple constant $\delta t = 1/\Gamma$ was found sufficient to describe the overall kinetics.

By repeating the kMC simulations a large number of independent trajectories, the results can be averaged to yield a statistical description of the complete relaxation pathway as a function of time. The total emission spectra are notably obtained by integrating the trajectory until no more relaxation events are possible.

E. Computational details and structural selection

All ingredients needed for the above calculations were provided by dedicated electronic structure calculations based on the SCC-DFTB method[15] for ground state vibrational energies and intensities of normal modes. Its time dependent version, which is referred to as TD-DFTB,[16] was used to determine vertical electronic state energies and oscillator strengths, computed for transitions from the ground electronic state exclusively. This approach was found to be able to determine both vibrational[11] and electronic[12] spectra of chemically diverse carbon clusters, and is thus found to be appropriate here for evaluating the intensity strengths and the vibrational densities of states, which were numerically calculated using the Beyer-Swinehart algorithm.[88] SCC-DFTB vibrational frequencies and TD-DFTB excitation energies were scaled[11,12] and 10^5 independent kMC trajectories were considered for each case.

Our objective is to unravel the relative efficiencies of RF and VE mechanisms in the radiative cooling of carbon clusters. Of special interest are the combined influences of size and structural features. In the present work, we considered sets of isomers for C_n (n=60, 42, 24) belonging to the four families mentioned in the introduction (cages, flakes, pretzels, branched). About 100 000 isomers per family were optimized at the SCC-DFTB level for C_{60}. Among those, we determined a subset of 1000 isomers per family for which the root mean square deviation (RMSD) of the families' order parameters (sp^2 fraction and asphericity parameter β) were the closest to the average value for the given family. The full sets of isomers will be considered in section IV. However, our first study is dedicated to individual isomers. We therefore first selected four isomers of C_{60} belonging to the cages, flakes, pretzel, and branched families, respectively, as well as two other members of the flakes family but having 24 or 42 atoms only.

These specific isomers, depicted in Fig. 1, were selected so that their average electronic and vibrational oscillator strengths are the closest to the average of the same quantities among the entire family set.

These properties are reported in Table I. Here we should emphasize that we purposely did not choose the buckminsterfullerene isomer of the cage family, which owing to its very particular symmetry is actually poorly representative of its own family. For instance, its lowest allowed electronic excited state lies more than 3 eV above the ground electronic state,[89] yielding essentially no recurrent fluorescence under the conditions where the other, less ordered isomers contribute to a much greater extent.

III. KINETICS OF RADIATIVE COOLING IN CARBON CLUSTERS: SELECTED CASES

A. Emission spectra

The total emission spectra of the six selected species were computed for a radiative cascade initiated from an excitation arbitrarily fixed at an internal energy 12.4 eV. These spectra are shown in Fig. 2. In the following, we discuss the influence of the different parameters on the competition between RF and VE. Regarding RF from an electronic excited state, its intensity depends on the electronic state energy, but also on

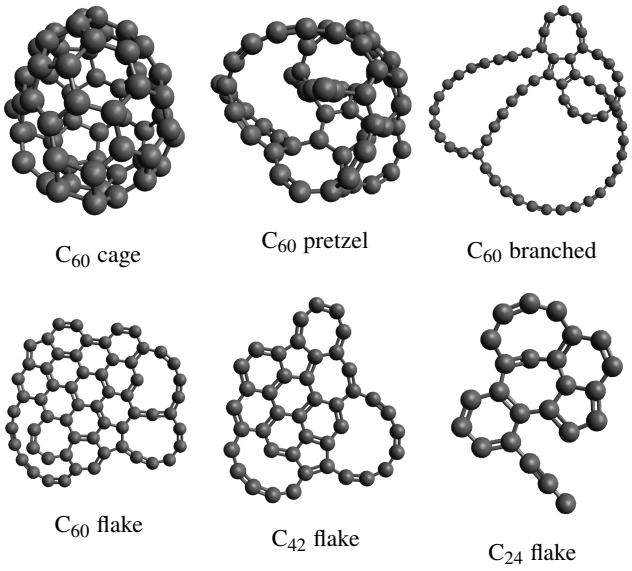

FIG. 1: Archetypal isomers of carbon clusters for all families and sizes.

Property	C_{60} cage	C_{60} pretzel	C_{60} branched	C_{60} flake	C_{42} flake	C_{24} flake
$\sum_{}^{50} f_{\text{elec}}$	0.14	0.22	1.34	0.26	0.31	0.23
$\sum I_{\text{vib}}$ (km/mol)	990	3300	7424	5600	3530	3260
$\overline{\omega}$ (cm^{-1})	754	537	372	559	557	557
ZPE (eV)	9.4	8.1	7.3	8.4	5.8	3.1
E_1 (eV)	0.25	0.33	0.27	0.21	0.26	0.60
E_2 (eV)	0.53	0.48	0.36	0.31	0.39	0.83
E_3 (eV)	0.58	0.76	0.66	0.35	0.50	0.95

TABLE I: Main features for the six selected carbon clusters, from top to bottom: sum over the first fifty electronic oscillator strengths (for all isomers, the 50$^{\text{th}}$ electronic state energy is less than 3 eV above that of the ground state), summed vibrational intensities, geometrical mean of vibrational wavenumbers, zero-point energies and energies of the three lowest excited electronic states.

the oscillator strengths of the involved transitions. The sum of the oscillator strengths over the fifty electronic states for all considered isomers is reported in Table I. The reported values for C_{60} illustrate the dependence on structure. More insight is provided by considering size effects. Comparing the RF from the C_{24}, C_{42} and C_{60} flake isomers, interesting variations can be noticed, which can be related to the density of electronic states. For such aromatic isomers, the density of electronic states increases with size (see Supplemental Material, Fig. S2), which leads to lower energies and more efficient RF processes. This can be explained by noticing that the larger the cluster, the higher the density of electronic states and the lower in energy are the first excited states. This trend is expected for such aromatic species, because the π electrons can be approximately considered as free in a spatially limited constant potential. By analogy with a particle in an infinite well, the more extended is the cluster, the broader is the well and the lower are the electronic energies.[90,91] In contrast, and while the number of vibrational modes also increases, their frequencies are limited on the high-frequency side by the carbon-carbon bond strength, which does not scale with cluster size but remains approximately constant (≈ 2100 cm^{-1}). Therefore, RF appears to be increasingly competitive with VE when the size of the isomer increases. It should also be noticed that C_{24} exhibits a particularly intense peak in the mid-IR region near 2000 cm^{-1}, which is a consequence of this structure having a terminating C_3 dangling chain (see Fig. 1) with a strongly varying dipole moment, leading to a particularly active IR response for this specific system, as seen in Table I on the summed IR intensity strength, which competes with that of the larger C_{42} cluster.

The dependence on structural type for a given size can also be examined by considering the four isomers chosen for C_{60}, assisted by the data reported in Table I. However, unlike size effects for the chemically similar flake isomers, the effects of structural type are not as clear. Still, it is worth noting that the RF and VE contributions to the emission spectrum are the most distinguishable from one another for the more disordered pretzel and branched isomers, the spectrum obtained for the cage structure presenting the same extent of overlapping between its electronic and vibrational parts.

B. Recurrent fluorescence and vibrational emission rate constants

Fig. 3 shows the variations of the total RF and VE rate constants, respectively for the 6 selected clusters, as a function of their internal energy. At low internal energies $E < 2.5$ eV the relative values of the RF constants for the 6 chosen clusters can be rationalized by both their relative density of electronic states below this energy and their oscillator strengths. At high energy, $E > 12.5$ eV, the density of states being similar for all clusters (Fig. S2), the relative rate constants can be accounted for by the oscillator strengths only. We discuss this in more detail below.

For an excess energy <2.5 eV, the total RF rate constant is particularly high for the cage and flake isomers of C_{60}, which is due to these isomers having their first electronic states lower in energy than the other two pretzel and branched isomers (see Table I). The particularly low total RF rate constant of the branched isomer of C_{60}, despite the first excited electronic state being as low as 0.27 eV, is explained by its very low vibrational frequencies as well (the lowest at 7 cm^{-1}), which makes the vibrational density of states increase more rapidly with internal energy and, in turn, leads to a slower increase of the excited electronic state occupation probability [see Eq. (6)], hence a lower RF rate constant than for the cage isomer of C_{60}.

We can then speculate at this stage that the positions of the first electronic states drive the evolution of the total RF rate constant at low internal energies. However, in some isomers the electronic oscillator strength of these first electronic states may be decisive for the value of the total RF rate constant at

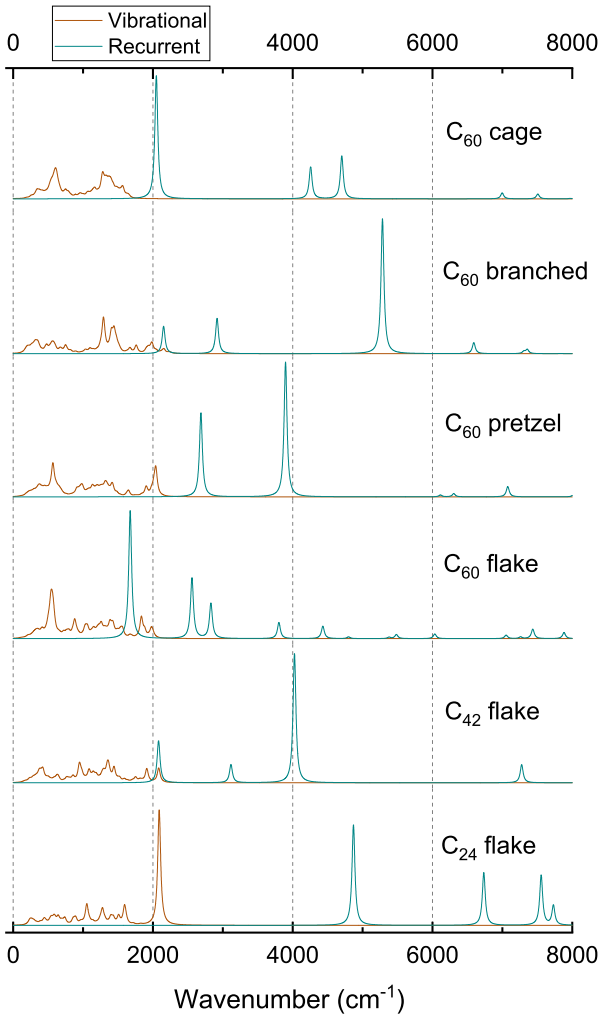

FIG. 2: Normalized emission intensity spectra of the six selected carbon clusters, as obtained from radiative cooling with 12.4 eV initial internal energy. The spectra were obtained as histograms and convoluted by a Lorentzian distribution with a full width at half maximum of $50\,\mathrm{cm}^{-1}$.[92–94]

low internal energies. An example of this behavior is provided by comparing the total RF rate constant of the branched and the pretzel isomers. At low internal energies, the pretzel conformer has a total RF rate constant slightly higher than the rate constant of the branched conformer despite its first electronic levels being much higher. This particular situation is explained by the relative electronic oscillator strengths involved in the process. According to our SCC-DFTB calculations, the oscillator strengths associated with the first and second electronic states of the pretzel and branched isomers are in the approximate ratios 1.1:0.4 and 4.9:1. This explains why RF is more efficient for the pretzel isomer.

At high internal energies $E > 12.4$ eV, the electronic oscillator strengths dictate the total RF rate constant because the energy of all electronic states is essentially the same for all clusters, whichever the family they belong to. The reason is that the electronic density of states for electronic energies below 2 eV above the ground state is approximately equal for all the C_{60} isomers, except for cages (see Fig. S2).

In particular, the higher electronic oscillator strengths, the higher the total RF rate constant. The branched isomer has higher electronic oscillator strengths than isomers from other families, further supporting this view. Conversely, the cage isomer is associated with a relatively low total RF rate constant that concurs with a relatively low electronic oscillator strength (see figure (3) and Table I for the selected species) and also with a slightly lower electronic density of states (fig. S2).

Size effects are also important on the magnitude of the total RF rate constant and its variations with increasing internal energy. For the specific flake family, from which members were selected for C_{24}, C_{42} and C_{60}, Fig. 3 shows that below 2.5 eV internal energy, the total RF rate constant of C_{60} exceeds that of C_{24} (and that of C_{42}). However, the rate of variations is also much steeper for the smaller cluster. This is a consequence of its reduced ability for storing energy, which is intimately related to the fewer degrees of freedom of C_{24}. Moreover, RF is efficient only if the electronic states are appreciably occupied and this occurs only if the quantity $\gamma = \rho(E - E_n)/\rho(E)$ is not negligible. Such a condition implies that vibrational excitation has to be high enough for the upper electronic states to be populated as well.

At high internal energies, the number of degrees of freedom also affects the total RF rate constant but in a much smoother way. The analysis of Sec. IIB shows that the main dependence on the number of degrees of freedom g occurs through the exponential term in the right hand side of Eq. (10), the total RF rate constant decreasing for increasing g at fixed internal energy. As the internal energy becomes very high, the exponential term tends toward unity and the RF rate constant from the n^{th} excited electronic state tends to its electronic fluorescence rate constant.

Fig. 3 also shows the variations of the total VE rate constants with increasing internal energy for the same 6 clusters. The vibrational activity is mostly sensitive to the set of frequencies, which for simplicity we sum up in their geometric average, and the set of vibrational intensity strengths.

Fig. 3 shows that the cage and the branched isomers of C_{60} are associated with the lowest and the highest VE rate constants for this stoichiometry, respectively. These differences can be understood from looking at the properties of the isomers in Table I: the intensity strength appears to be the lowest for the cage, while the average vibrational frequency is the highest, implying fewer quanta at a given internal energy. The same arguments can be used to explain the opposite behavior of the branched isomer and its particularly high VE rate constant.

Size effects are also marked for VE processes, and remain the manifestation of fewer quanta being distributed in the various vibrational modes at fixed internal energy. As expressed by Eq.(12), the VE rate constant is expected to decrease with increasing g, at fixed E. In Fig. 3 the VE rate constant for the

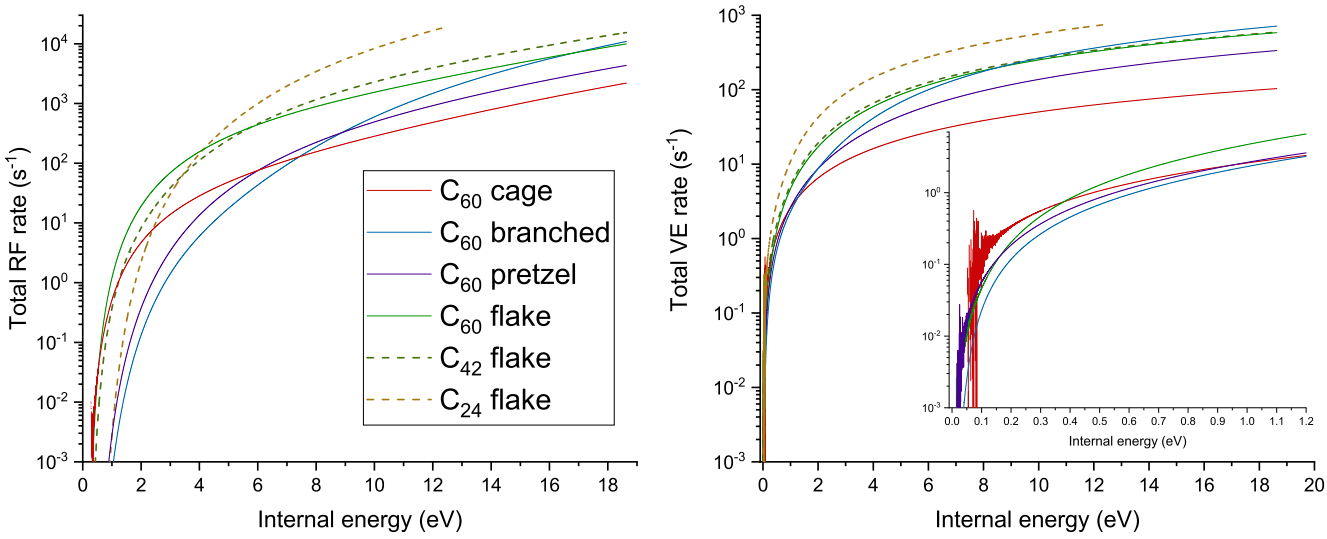

FIG. 3: Left panel: Recurrent fluorescence rate constants for the six selected carbon clusters, as a function of their internal energy. Right panel: Vibrational emission rate constants for the six selected carbon clusters, as a function of their internal energy. The inset focuses on the low internal energies below 1.24 eV.

C_{42} flake isomer indeed lies between the corresponding rate constants for the two other flake isomers C_{24} and C_{60} at low energies, but crosses that of C_{60} at high energies. As seen in Table I, this specific behavior is partly fortuitous as it results from the unexpectedly low average intensity strength for this system, very close to the value in C_{24}.

C. Quantifying the competition between RF and VE processes

Having neglected electronic fluorescence, thermal dissociation and delayed ionization, the competition between RF and VE mechanisms can be directly quantified from the ratio of their rate constants:

$$\xi(E) = \frac{A_{\rm rec}^{\rm tot}}{A_{\rm rec}^{\rm tot} + A_{\rm vib}^{\rm tot}}. \qquad (15)$$

The variations of this quantity with increasing energy are shown in Fig. 4 for the 6 selected clusters. At low energy, VE is the main mechanism for all systems. Then ξ increases monotonically with internal energy and ranges from 0 at low energies and eventually exceeds 90% above 17.5 eV, indicating that RF becomes the increasingly dominant process at very high energies.

The value of the RF efficiency ξ and its variations from one isomer to another can be rationalized again from the electronic oscillator strengths and the vibrational activities. The particularly low electronic levels of the C_{60} cage and flake isomers cause their RF efficiency to increase from an internal energy as low as 1.24 eV. Their increase is steeper than that of the two other isomers of this size, but this is due to two distinct effects. In the case of the flake isomer, RF is particularly strong, while VE is very inefficient for the cage. For the branched isomer, vibrational frequencies are particularly low (22 vibrational frequencies below 100 cm^{-1} and the lowest is at 7 cm^{-1}) as shown by the value of the geometrical mean of vibrational frequencies (Table I), making the RF rate constant lower despite its first electronic state being similar to that of the cage isomer: low vibrational frequencies imply higher vibrational densities of states and thus lower excited electronic state occupation probabilities [see Eq. (6)].

In general, the isomer size also has an effect on the overall evolution of the RF efficiency. At low energy, larger isomers are associated with lower electronic states energies, leading to higher total RF rate constants. The RF efficiency then increases and reaches a maximum value at lower internal energies. Even though the RF efficiency for C_{24} increases at higher internal energies, it reaches its maximum value earlier than for both C_{42} and C_{60}, the three efficiencies crossing each other near 6.2 eV. The reason behind this size effect is again to be found in noticing that, for a fixed internal energy, smaller clusters are warmer because of the fewer degrees of freedom in which this excess energy can be shared. At low internal energy, smaller clusters thus have a higher fraction of this energy available for recurrent fluorescence, hence a lower associated rate constant. At high internal energy, where electronic and vibrational components can flow both ways more easily, RF efficiency becomes stronger for smaller clusters because the vibrational degrees of freedom play a relatively less important role.

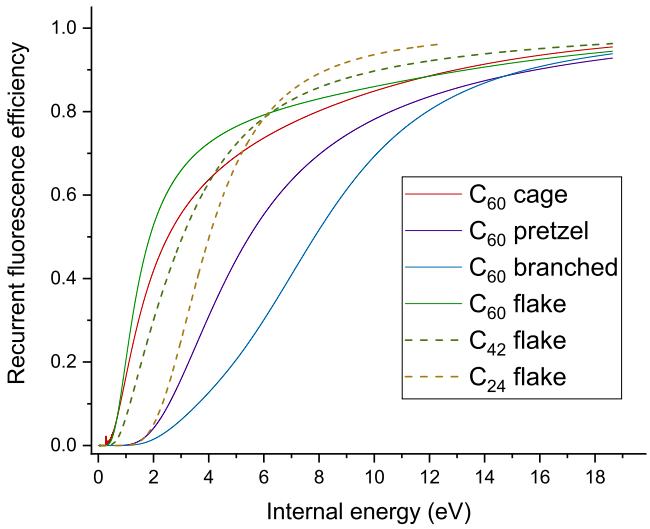

FIG. 4: Recurrent fluorescence efficiency ξ obtained from the rate constants of figure 3.

D. Kinetics of radiative cooling

We turn now to the kinetics of radiative cooling processes in more detail, to discuss the decay of the internal energy initially deposited into the system.

Using the kinetic Monte Carlo procedure described in Sec. II, the flow of energy in the system between the various electronic and vibrational degrees of freedom can be monitored as a function of time. Fig. 5 displays the variations of the total energy in the six clusters as a function of time, for an excess energy of 18.5 eV in all systems; the statistics are accumulated over 10^5 independent kMC trajectories.

From this graph, plotted in double logarithmic scale, it appears that for some isomers the internal energy decays in a piece-wise linear fashion. If we arbitrarily define a relaxation time as the duration needed for the internal energy to decrease by a factor of 10, we find values between 0.1 and 1 s depending on the size and isomer type.

The different slopes in the various curves are the manifestations of different relaxation regimes in which the dominant mechanism varies along the relaxation path. A more detailed example is discussed in Fig. 5 for the flake isomer of C_{60}, in conjunction with Fig. 6 where the four main relaxation regimes are highlighted. The first relaxation regime, occurring at short times and for energies still located above 12.4 eV, is correlated with the presence of five competing relaxation pathways involving recurrent fluorescence, in particular first, second, third, twelfth and thirteenth electronic states (see Fig. 6). Once the energy drops to 8.7 eV, recurrent fluorescence from the twelfth and thirteenth electronic levels become negligible and this corresponds to another decay regime, denoted as the second regime, located between 7.4 and 3.1 eV. As the internal energy drops below 3.1 eV, RF becomes efficient when the first electronic state is involved, which is associated with yet another decay regime (third regime) between 2.5 and 1 eV. Finally, below 0.75 eV, RF from the first electronic excited state becomes negligible compared to VE processes, leading to another, fourth regime. The time dependence of RF and VE competition can be analyzed by putting together Figs. 4 and 5. For the C_{60} flake, the RF efficiency is less than 0.5 for internal energies below 1.9 eV and for times beyond 0.2 s during which RF occurs only from the first excited electronic state (Fig. 6).

Comparing now the behaviors for the various isomers, and keeping in mind that RF is the dominant process at high energies, relaxation in the branched isomer is slightly faster than in the 60-atom flake, although this is not immediately obvious in Fig. 5. This is concomitant with the higher RF rate for the branched isomer. However, below 10 eV relaxation in the C_{60} flake is faster because its RF rate constant is much higher than others while the RF rate constant of the C_{60} branched isomer is reduced owing to the high first electronic levels of this isomer (see Fig. 3). Below 2.5 eV, the cage isomer relaxes faster than the branched and pretzel isomers because their RF rate constants are particularly low. This is not the case for the flake and cage isomers owing to their low-lying electronic states. The faster decrease obtained for the cage isomer compared to the flake compound is due to the VE process being dominant at energies lower than 0.4 eV, and which is favored also for the cage isomer relative to the flake (see inset in Fig. 3).

As shown in Sec. III C, the RF efficiency increases with internal energy whatever the size and the family of the isomer. Fig 2 shows that RF usually emits higher energetic photons. Smaller isomers have a higher RF efficiency at high internal energies and thus their radiative relaxation is faster for smaller isomers (Fig. 5). Even at low internal energy, where RF is poorly efficient, radiative relaxation is faster for smaller iso-

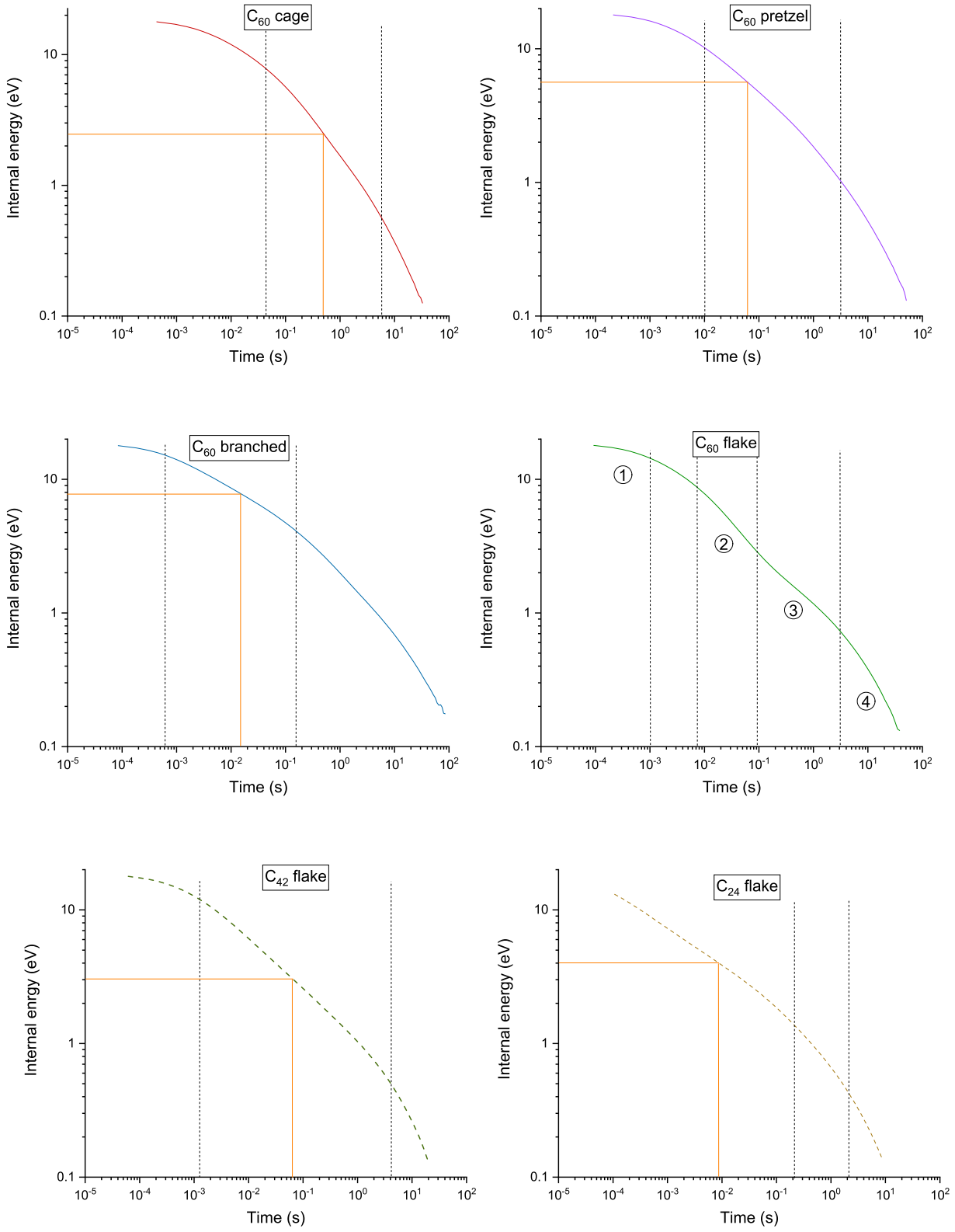

FIG. 5: Temporal decay of the internal energy for the six carbon clusters. For all isomers, the initial internal energy was set to 18.5 eV except for the C_{24} flake for which it was only 14.9 eV. Main regime shifts are highlighted by vertical dashed lines. The numbering in circles for the C_{60} flake decay curve indicates the main decay regimes. Orange lines indicate the internal energy and the delay for which the RF efficiency is 0.5 (as deduced from Fig. 4).

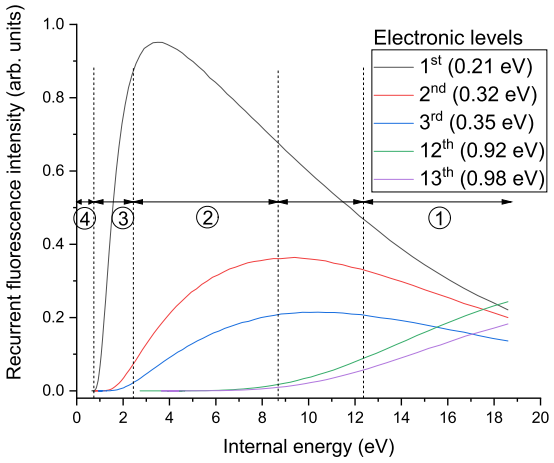

FIG. 6: Recurrent fluorescence intensities from dominant electronic states as a function of the internal energy for the C_{60} flake. The numbering in circles indicates different relaxation regimes.

mers because, at fixed energy, vibrational quantum numbers are higher and thus the VE rate constant is higher. As far as structural dependence is concerned, our study also indicates that there is no clear general tendency but, conversely, that relaxation processes depend significantly on the isomers structures. More insight into these aspects can be gained from looking at broader sets of structures.

IV. BEHAVIOR OVER A LARGE SET

We now extend our scope by attempting to correlate the fluorescence rate constants with the structural features of the carbon clusters, beyond the limited examples scrutinized in Sec. III.

A. Electronic gap law decay type for RF rate constants

For simplicity, we assume that a single excited electronic state is available for all clusters. Its recurrent fluorescence rate constant in Eq. (7) can be expressed more explicitly by employing the semiclassical harmonic approximation of Eq. (9). The corresponding rate constant is straightforwardly obtained by applying Eq. (10) with $n_{\max} = 1$:

$$A^1_{\rm rec} = A^1_f e^{-\frac{g-1}{E+E_z}E_1}, \qquad (16)$$

where, consistent with the semiclassical approximation, we have further used $E_1 \ll E + E_z$. In Eq. (16), the internal energy E can be viewed as a parameter of the RF rate constant.

We have determined the corresponding quantity for much larger sets of structures for which the low-lying electronic excited states are available,[12] namely one thousand isomers for each of the four families of C_{60}, as well as one thousand flake isomers for each of the smaller C_{24} and C_{42} systems. The RF rate constants obtained through kMC simulations for these six sets of isomers and for different values of the internal energy are shown as scattered plots in Fig. 7.

For each system, the logarithm of the RF rate constant varies roughly linearly with the first electronic excited state energy at sufficiently high energies, confirming the exponential relation of Eq. (16). This exponential behavior is particularly clear in the case of C_{60} cage isomers, for which the RF rate constant was determined at four internal energies, the results being shown in the upper left part of Fig. 7. In this case, the linear part in the logarithmic RF rate constant is well established once the electronic energy lies above 0.2 eV. We can correlate the quality of the exponential dependence by performing a linear regression of the logarithmic rate constant for electronic energies in the above range and estimating the corresponding Pearson correlation factor R. At internal energies below 12.4 eV this factor is the range of 53–96%, while it drops to 6% at the higher internal energy considered.

The slope of the linear fit of the scatter plots tends to 0 with increasing internal energy, which is explained by the exponential in Eq. (16) approaching unity in this regime. Thus, the scatter plots tend to the electronic fluorescence values for very high internal energies. At lower electronic energies, the strong increase in the RF rate constant reflects the concomitant increase in the electronic oscillator strength. A similar dependence is also predicted for the other electronic states of all isomers, with comparable exponential variations since the slope in logarithmic scale only depends on the size of the system and its internal energy. This behavior is illustrated in Fig. 7b where the RF rate constants obtained for C_{60} cage isomers and excitations on the first or second electronic states are represented against the corresponding energy, at the two internal energies of 0.62 and 6.2 eV: the exponential rate of variations does not depend on the electronic state from which fluorescence originates, but only on internal energy.

The size dependence is better examined by comparing the RF rate constants obtained for the various flake isomers of the three different clusters, for a fixed electronic excitation state and a fixed internal energy. The resulting total RF rate constants determined for such samples of C_{24}, C_{42} and C_{60} are shown in Fig. 7c. From this figure the slope in the logarithmic scale is found to decrease with decreasing size [see Eq. (16)]. However, these slopes do not scale linearly with the term $\frac{g-1}{E+E_z}$, as Eq. (16) would suggest. From Fig. 7c and Eq. (16), the ratios between the slope and the corresponding term $\frac{g-1}{E+E_z}$ vary as 1.14(C_{24}):1.11(C_{42}):1(C_{60}). We interpret this discrepancy as due to the condition $E + E_z \gg E_1$ necessary for Eq. (16) but not completely valid for all C_{24} and C_{42} isomers at 1.24 eV internal energy. These ratios tend to unity with the internal energy and at 2.5 eV internal energy they read as 1.08(C_{24}):1.07(C_{42}):1(C_{60}) (see Supplemental Material, Fig. S3). Fig. 7d shows RF rate constants from the first electronic states for flake and cage isomers. The overall shape of the scatter plot remains unchanged even if slight differences are seen due to the electronic levels of C_{60} flake isomers being lower than those of cage isomers.

The exponential decay dependence of the RF rate constant from a given electronic level is similar to the energy gap law decay (EGL) encountered in radiationless transitions, which states that the non-radiative (internal conversion or intersystem crossing) rate constant from an upper electronic level to a lower level decreases as $e^{-\beta\Delta E}$ with ΔE the energy gap between the two electronic states.[66] Such an exponential dependence originates from the couplings between the electronic state and the vibronic states of other electronic states. These are proportional to Franck-Condon factors, which present an exponential decay with the electronic gap,[65] itself determined by the accepting modes of the vibrational energy reservoir. Here, the origin of the term $e^{-\frac{g-1}{E+E_z}E_1}$ is exactly the same as that of the Boltzmann factor in the canonical framework. The overall internal energy can therefore be viewed as an energy reservoir by the electronic level being occupied, as long as it is negligible against internal energy. In this case, there is an analogy between the quantity $\frac{E+E_z}{g-1}$ appearing in the exponential decay and the well-known thermal energy k_BT.

B. Global emission spectra

The effects of isomer diversity can also be examined by their emission spectra resulting from a cascade of successively emitted photons, as modeled using the kinetic Monte Carlo approach described in Sec. IIB. Following a similar approach to previous work[95,96] we determined the emission spectra of entire samples of isomers by summing the individual contributions of all their members (independent of each other as in the gas phase), with uniform weighting. The initial internal energy is the same for all isomers. The emission spectra were determined assuming either vibrational emission only, or including also the contribution of recurrent fluorescence.

The upper panels of Fig. 8 show the emission spectrum resulting from the sample of 1000 cage isomers of C_{60} excited at 2.5 eV and 12.4 eV energies, respectively. The RF spectra span a broad range of wavenumbers, usually starting around 500 cm^{-1}, and overlap with the VE spectra. RF seems also rather weak compared to VE in the region where VE dominates (below 2000 cm^{-1}), which could seem somewhat contradictory with our earlier conclusion that RF efficiency is significant, especially at the higher internal energy considered. However, it is important to recognize that the density of vibrational states is much higher than the corresponding density of electronic states in the overlap region, and this effect is further magnified by the statistical averaging over the 1000 isomers (Figs. S4, S5, and S6), which leads to a nearly continuous distribution of vibrational modes in the 0–2000 cm^{-1} range, while the electronic states are much fewer and fall into much narrower distributions. Moreover, once VE becomes significant it quickly drains internal energy away from the system and quenches the possibility of RF, making it even less likely.

These processes contribute to partitioning the overall emission spectra and showing an overlapping region between the two ranges in which either of the two processes is clearly dominant. At both internal energies, the overall RF spectral profile shows a bell shaped profile with an extended high frequency wing. The sharp increase at low electronic energy is due to the square dependence of electronic fluorescence rate constant on electronic energy expressed in Eq. (4) and to the increase of the electronic density of states (Figs. S3, S4 and S5). The decrease at high energies is found to be exponential, and can be essentially understood from the EGL type behavior of the RF rate constants, even though the global spectrum obtained here results from an emission cascade and the contribution from multiple isomers.

The global emission spectra obtained for the other structural families of C_{60} are depicted in the lower part of Fig. 8, at the same two internal energies of 2.5 and 12.4 eV, and together with the spectra discussed above for the cage isomers. For the other three families, a vibrational emission band is seen above 2000 cm^{-1}, as originating from chains of sp carbon atoms that are mostly absent in the cages. Broad bands found between 1600 cm^{-1} and 1000 cm^{-1} are essentially due to CC stretching modes possibly overlapping with CCC bending modes near 1000 cm^{-1} (Ref. 11). Broad bands around 600 cm^{-1} involve CCC in-plane and out-of-plane bending modes associated with stronger deformation of the overall structures.[11]

At 2.5 eV initial internal energy, the RF component of the global emission spectrum is not very strong for all the four structural families, especially for pretzels and branched isomers. This is consistent with our earlier observation in Fig. 4 that these structures have a particularly low RF efficiency. At 12.4 eV, the contribution of RF to the global spectrum is much stronger and affects the entire spectral range for all families. As the internal energy increases, the band ratios thus also vary as the result of the increasing importance of recurrent fluorescence. This effect is more pronounced for high frequency modes, which can be interpreted by the high energy approximation of Eq. (12):

$$A_i(E) = A_i^{1\to 0}\frac{E}{g\hbar\omega_i} \propto \omega_i^2 f_i \frac{E}{g}. \tag{17}$$

The influence of RF processes on the VE emission spectra thus amounts to inhibitting emission from high vibrational frequency modes, where the competition with the low-lying electronic states is the strongest. High frequency vibrational modes are therefore less likely to emit photons when RF is accounted for, which precisely matches our computational results.

V. CONCLUDING REMARKS

Upon initial excitation, isolated large carbon clusters may relax through recurrent fluorescence and vibrational emission processes, whose relative efficiency was found here to depend on a number of factors. The present work aimed at elucidating this dependence by means of dedicated modeling, systematically addressing the roles of cluster size, structural features, and the excess energy itself.

For the present clusters containing several tens of carbon atoms, recurrent fluorescence was generally found to become important as soon as the internal energy exceeds about 1 eV,

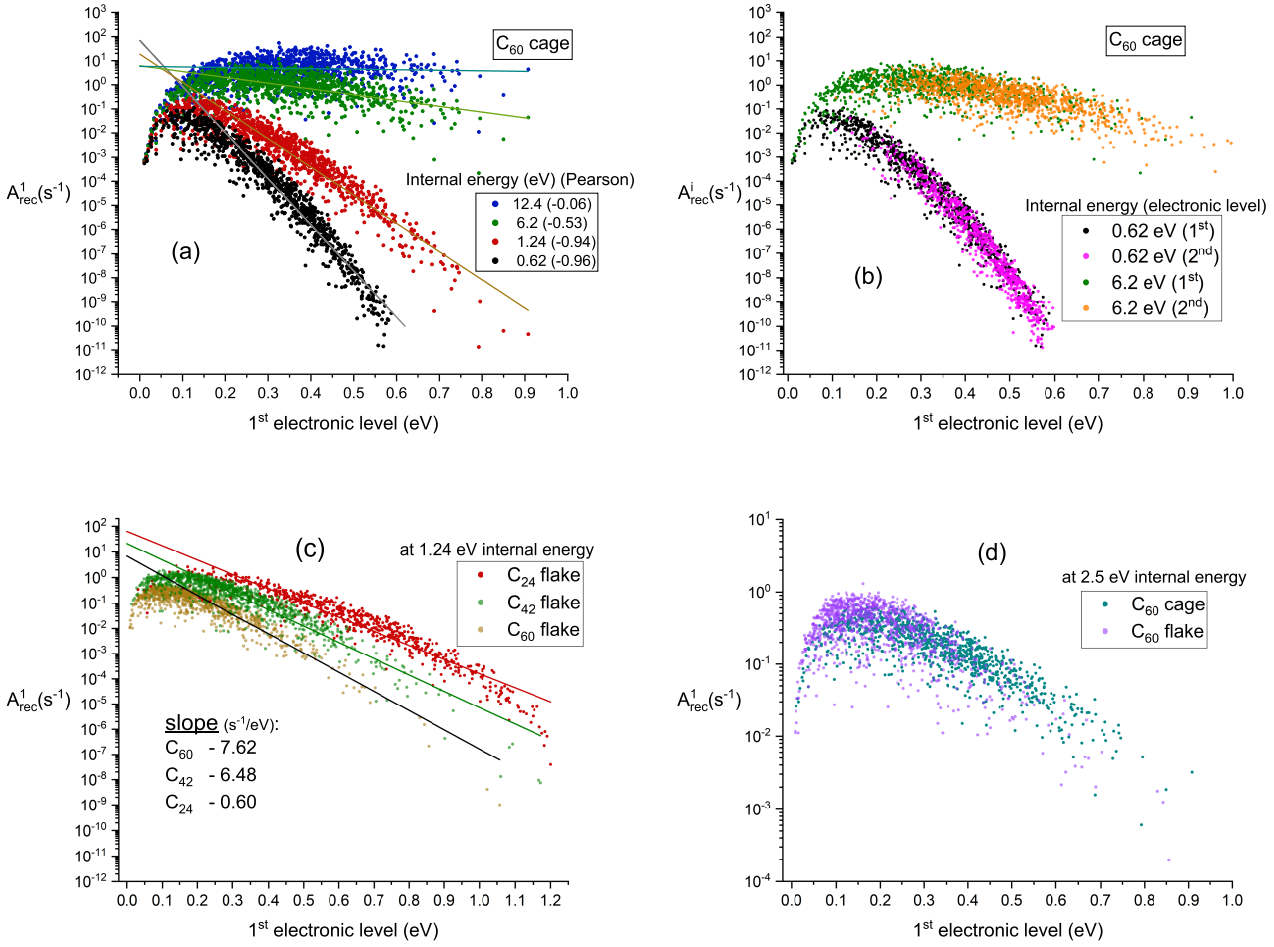

FIG. 7: RF rate constants for various isomers and internal energies, as a function of the position of the electronic excited state. (a) from the 1st electronic level for several internal energies of C_{60} cage isomers. The lines are the best linear fits determined for data above 0.2 eV with Pearson factors given in the inset; (b) from the 1st or 2nd electronic level at two internal energies for C_{60} cage isomers; (c) from the 1st electronic level for C_{24}, C_{42} and C_{60} flake isomers; (d) from the 1st electronic level for C_{60} cage and flake isomers.

even dominating over vibrational emission above 10 eV. The very high efficiency of recurrent fluorescence identified at high internal energies is not only due to the appreciable occupation of excited electronic states but also to their significant electronic oscillator strength, which is typically two or three orders of magnitude larger than vibrational intensities.

At low or moderate internal energies, a significant dependence of recurrent fluorescence efficiency on the structural family was also found, such electronic processes being more exacerbated for flakes owing to their low-lying electronic states. Cages also show a higher RF efficiency, but as the result of their lower vibrational activity. The size dependence of recurrent fluorescence is also substantial at low internal energies (below 7.4 eV), in relation with their reduced ability to store vibrational energy.

From the spectral viewpoint, the recurrent fluorescence spectra obtained from an emission cascade is constituted of a main emission band that becomes increasingly broad with increasing internal energy. The intensity increase in the RF spectrum at low energies originates from the concomitant increase in the propensity for spontaneous emission with electronic transition energy, given that these states are appreciably occupied. Similarly, the decrease at high energies results from the exponentially decaying occupation probabilities.

When considering populations of isomers, the recurrent fluorescence rate constant from a given electronic state was found to follow a behavior similar to the energy gap law decay in radiationless transitions. This was interpreted as resulting from the numerous degrees of freedom in the present clusters, whose vibrational energy distribution is perceived as a statistical reservoir from the perspective of an electronic excitation. Recurrent fluorescence also has a noticeable influence on vibrational emission spectra by inhibiting high vibrational frequency modes. In this spectral region, recurrent fluores-

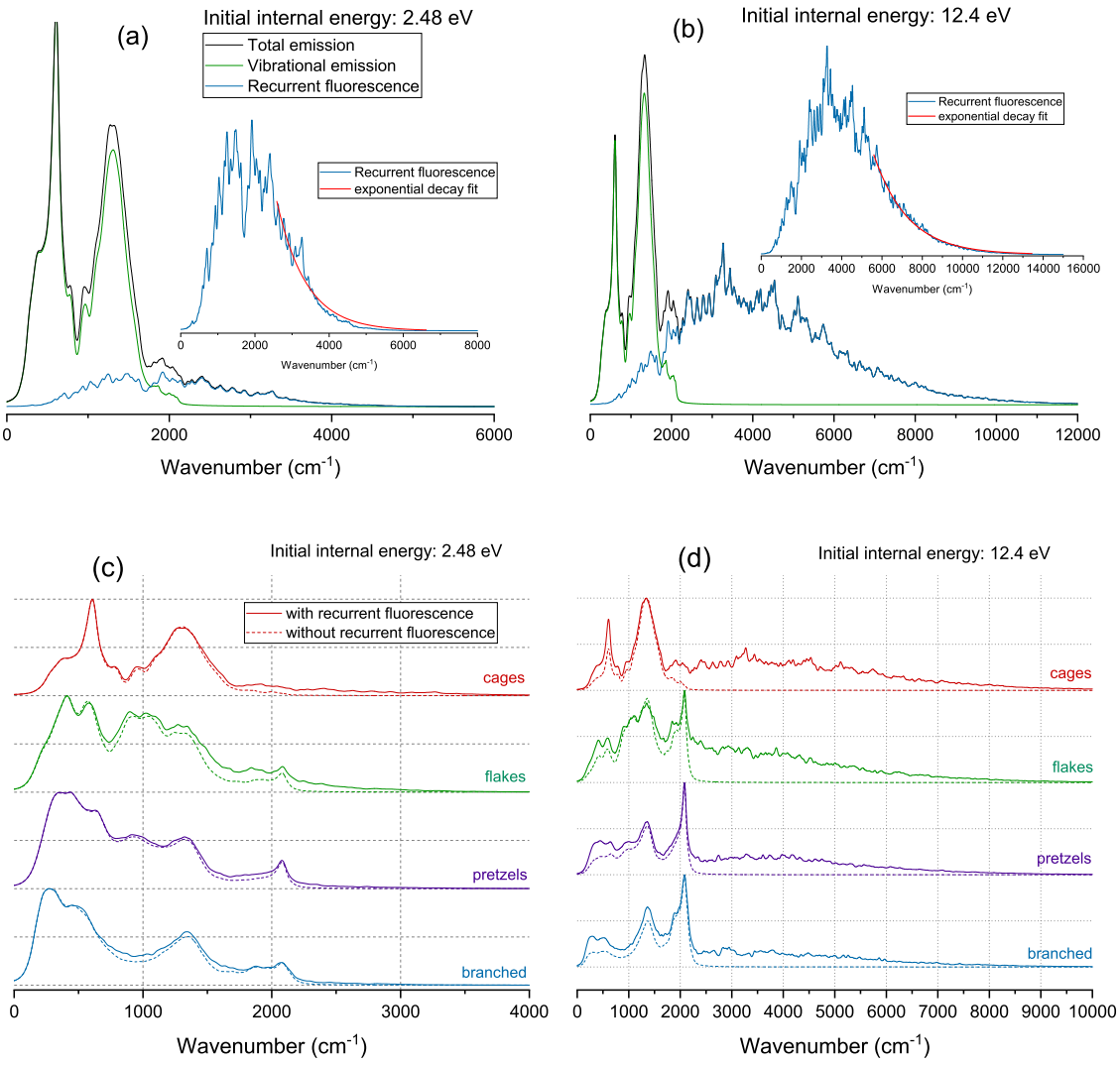

FIG. 8: (a) and (b): Normalized emission intensity spectra from one thousand isolated C_{60} cage isomers with 2.5 and 12.4 eV initial internal energy. Contribution from recurrent fluorescence and vibrational emission are also displayed. The inset highlights the exponential fit for the recurrent fluorescence component; (c) and (d): Normalized emission intensity spectra from one thousand isolated C_{60} isomers for each family. Spectra in dashed lines (resp. solid lines) are those without (resp. with) recurrent fluorescence taken into account over the relaxation cascade.

cence tends to attenuate the band ratio between high and low frequency vibrational modes.

SUPPLEMENTARY MATERIAL

The Supplementary Material contains four sections. The section A is dedicated to the estimation of the corrected γ_n quantity in Eq. 6 when the approximation $\rho_n(E-E_n) \approx \rho_0(E-E_n)$ is not assumed. The conclusion is that the correction on γ_n is usually less than 10 %. In section B, the electronic density of states of the six chosen isomers are shown. In section C, the recurrent fluorescence rate at 2.5 eV internal energy for flake isomers is shown to compare the slopes with analytical expressions in Eq. 7. Section D concerns the electronic density of states and number of vibrational modes over a large set of isomers for the four families and the three sizes.

DATA AVAILABILITY STATEMENT

The data that support the findings of this study are available from the corresponding author upon reasonable request.

ACKNOWLEDGMENTS

This work has been supported by the ANR project PACHYNO (ANR-16-CE29-0025).

[1] H. Handschuh, G. Ganteför, B. Kessler, P. S. Bechthold, and W. Eberhardt, Phys. Rev. Lett. **74**, 1095 (1995).
[2] A. Van Orden and R. J. Saykally, Chem. Rev. **98**, 2313 (1998).
[3] S. K. Lai, I. Setiyawati, T. W. Yen, and Y. H. Tang, Theor. Chem. Acc. **136**, 20 (2016).
[4] M. A. Bonnin, C. Falvo, F. Calvo, T. Pino, and P. Parneix, Phys. Rev. A **99**, 042504 (2019).
[5] G. Von Helden, M.-T. Hsu, P. R. Kemper, and M. T. Bowers, J. Chem. Phys. **95**, 3835 (1991).
[6] G. von Helden, M. T. Hsu, N. Gotts, and M. T. Bowers, J. Chem. Phys **97**, 8182 (1993).
[7] N. G. Gotts, G. von Helden, and M. T. Bowers, Int. J. Mass. Spectrom. Ion Process **149–150**, 217 (1995).
[8] A. A. Shvartsburg, G. C. Schatz, and M. F. Jarrold, J. Chem. Phys. **108**, 2416 (1998).
[9] J. M. Hunter and M. F. Jarrold, J. Am. Chem. Soc. **117**, 10317 (1995).
[10] M. T. Bowers, Int. J. Mass Spectrom. **370**, 75 (2014).
[11] C. Dubosq, C. Falvo, F. Calvo, M. Rapacioli, P. Parneix, T. Pino, and A. Simon, Astron. Astrophys. **625**, L11 (2019).
[12] C. Dubosq, F. Calvo, M. Rapacioli, E. Dartois, T. Pino, C. Falvo, and A. Simon, Astron. Astrophys. **634**, A62 (2020).
[13] D. W. Brenner, O. A. Shenderova, J. A. Harrison, S. J. Stuart, B. Ni, and S. B. Sinnott, J. Phys. Cond. Mat. **14**, 783 (2002).
[14] S. G. Kim and D. Tománek, Phys. Rev. Lett. **72**, 2418 (1994).
[15] M. Elstner, D. Porezag, G. Jungnickel, J. Elsner, M. Haugk, T. Frauenheim, S. Suhai, and G. Seifert, Phys. Rev. B **58**, 7260 (1998).
[16] T. A. Niehaus, S. Suhai, F. Della Sala, P. Lugli, M. Elstner, G. Seifert, and T. Frauenheim, Phys. Rev. B **63**, 085108 (2001).
[17] J. F. Anacleto, H. Perreault, R. K. Boyd, S. Pleasance, M. A. Quilliam, P. G. Sim, J. B. Howard, Y. Makarvovsky, and A. L. Lafleur, Rapid Commun. Mass Spectrom. **6**, 214 (1992).
[18] V. M. Rotello, J. B. Howard, T. Yadav, M. M. Conn, E. Viani, L. M. Giovane, and A. L. Lafleur, Tetrahedron Lett. **34**, 1561 (1993).
[19] Q.-L. Zhang, S. C. O'Brien, J. R. Heath, Y. Liu, R. F. Curl, H. W. Kroto, and R. E. Smalley, J. Phys. Chem. **90**, 525 (1986).
[20] E. Dartois, J. Carb. Res. **5**, 80 (2019).
[21] K. Sellgren, M. W. Werner, J. G. Ingalls, J. D. T. Smith, T. M. Carleton, and C. Joblin, Astrophys. J. Lett. **722**, L54 (2010).
[22] J. Cami, J. Bernard-Salas, E. Peeters, and S. E. Malek, Science **329**, 1180 (2010).
[23] M. Otsuka, F. Kemper, S. Hyung, B. A. Sargent, M. Meixner, A. Tajitsu, and K. Yanagisawa, Astrophys. J. **764**, 77 (2013).
[24] Y. Zhang and S. Kwok, Astrophys. J. **730**, 126 (2011).
[25] K. R. G. Roberts, K. T. Smith, and P. J. Sarre, Monthly Not. Royal Astron. Soc. **421**, 3277 (2012).
[26] O. Berné, N. L. J. Cox, G. Mulas, and C. Joblin, Astron. Astrophys. **605**, L1 (2017).
[27] M. A. Cordiner, H. Linnartz, N. L. J. Cox, J. Cami, F. Najarro, C. R. Proffitt, R. Lallement, P. Ehrenfreund, B. H. Foing, T. R. Gull, *et al.*, Astrophys. J. Lett. **875**, L28 (2019).
[28] O. Berne, G. Mulas, and C. Joblin, Astron. Astrophys. **550**, L4 (2013).
[29] E. K. Campbell, M. Holz, D. Gerlich, and J. P. Maier, Nature (London) **523**, 322 (2015).
[30] J. P. Maier and E. K. Campbell, Angew. Chem. Int. Ed. **129**, 5000 (2017).
[31] A. O. Lykhin, S. Ahmadvand, and S. A. Varganov, J. Phys. Chem. Lett. **10**, 115 (2018).
[32] S. R. Federman, C. J. Strom, D. L. Lambert, J. A. Cardelli, V. V. Smith, and C. L. Joseph, Astrophys. J. **424**, 772 (1994).
[33] J. P. Maier, N. M. Lakin, G. A. Walker, and D. A. Bohlender, Astrophys. J. **553**, 267 (2001).
[34] P. F. Bernath, K. H. Hinkle, and J. J. Keady, Science **244**, 562 (1989).
[35] O. Berné and A. G. G. M. Tielens, Proc. Natl. Acad. Sci. U.S.A. **109**, 401 (2012).
[36] J. Zhen, P. Castellanos, D. M. Paardekooper, H. Linnartz, and A. G. G. M. Tielens, Astrophys. J. Lett. **797**, L30 (2014).
[37] P. W. Dunk, N. K. Kaiser, C. L. Hendrickson, J. P. Quinn, C. P. Ewels, Y. Nakanishi, Y. Sasaki, H. Shinohara, A. G. Marshall, and H. W. Kroto, Nat. Commun. **3**, 855 (2012).
[38] A. Leger and J. L. Puget, Astron. Astrophys. **137**, L5 (1984).
[39] L. J. Allamandola, A. G. G. M. Tielens, and J. R. Barker, Astrophys. J. **290**, L25 (1985).
[40] E. Kolodney, A. Budrevich, and B. Tsipinyuk, Phys. Rev. Lett. **74**, 510 (1995).
[41] J. U. Andersen, C. Brink, P. Hvelplund, M. O. Larsson, B. B. Nielsen, and H. Shen, Phys. Rev. Lett. **77**, 3991 (1996).
[42] K. Hansen and E. E. B. Campbell, J. Chem. Phys. **104**, 5012 (1996).
[43] J. U. Andersen, C. Gottrup, K. Hansen, P. Hvelplund, and M. O. Larsson, Eur. Phys. J. D **17**, 189 (2001).
[44] K. Hansen, J. U. Andersen, P. Hvelplund, S. P. Møller, U. V. Pedersen, and V. V. Petrunin, Phys. Rev. Lett. **87**, 123401 (2001).
[45] A. E. K. Sundén, M. Goto, J. Matsumoto, H. Shiromaru, H. Tanuma, T. Azuma, J. U. Andersen, S. E. Canton, and K. Hansen, Phys. Rev. Lett. **103**, 143001 (2009).
[46] K. Najafian, M. S. Pettersson, B. Dynefors, H. Shiromaru, J. Matsumoto, H. Tanuma, T. Furukawa, T. Azuma, and K. Hansen, J. Chem. Phys. **140**, 104311 (2014).
[47] H. Shiromaru, T. Furukawa, G. Ito, N. Kono, H. Tanuma, J. Matsumoto, M. Goto, T. Majima, A. E. K. Sundén, K. Najafian, *et al.*, in *J. Phys.: Conf. Ser.*, Vol. 635 (2015) p. 012035.
[48] N. Kono, R. Suzuki, T. Furukawa, J. Matsumoto, H. Tanuma, H. Shiromaru, T. Azuma, and K. Hansen, Phys. Rev. A **98**, 063434 (2018).
[49] F.-Q. Chen, N. Kono, R. Suzuki, T. Furukawa, H. Tanuma, P. Ferrari, T. Azuma, J. Matsumoto, H. Shiromaru, V. Zhaunerchyk, *et al.*, Phys. Chem. Chem. Phys. **21**, 1587 (2019).
[50] M. H. Stockett, J. N. Bull, J. T. Buntine, E. Carrascosa, E. K. Anderson, M. Gatchell, M. Kaminska, R. F. Nascimento, H. Cederquist, H. T. Schmidt, *et al.*, Euro. Phys. J. D **74**, 150 (2020).
[51] J. N. Bull, M. S. Scholz, E. Carrascosa, M. K. Kristiansson, G. Eklund, N. Punnakayathil, N. de Ruette, H. Zettergren, H. T. Schmidt, H. Cederquist, *et al.*, J. Chem. Phys. **151**, 114304 (2019).
[52] M. H. Stockett, J. N. Bull, J. T. Buntine, E. Carrascosa, M. Ji, N. Kono, H. T. Schmidt, and H. Zettergren, J. Chem. Phys. **153**, 154303 (2020).
[53] A. Léger, P. Boissel, and L. d'Hendecourt, Phys. Rev. Lett. **60**, 921 (1988).
[54] W. W. Duley, Astrophys. J. **705**, 446 (2009).
[55] T. S.-Y. Lai, A. N. Witt, C. Alvarez, and J. Cami, Mon. Not. R. Astron. Soc. **492**, 5853 (2020).
[56] T. S.-Y. Lai, A. N. Witt, and K. Crawford, Mon. Not. R. Astron. Soc. **469**, 4933 (2017).
[57] K. Sellgren, Astrophys. J. **277**, 623 (1984).
[58] R. Mitzner and E. E. B. Campbell, J. Chem. Phys. **103**, 2445 (1995).
[59] E. A. Rohlfing, J. Chem. Phys. **89**, 6103 (1988).
[60] S. Martin, J. Bernard, R. Brédy, B. Concina, C. Joblin, M. Ji, C. Ortega, and L. Chen, Phys. Rev. Lett. **110**, 063003 (2013).
[61] M. Saito, H. Kubota, K. Yamasa, K. Suzuki, T. Majima, and H. Tsuchida, Phys. Rev. A **102**, 012820 (2020).
[62] G. Ito, T. Furukawa, H. Tanuma, J. Matsumoto, H. Shiromaru, T. Majima, M. Goto, T. Azuma, and K. Hansen, Phys. Rev. Lett. **112**, 183001 (2014).
[63] V. Chandrasekaran, B. Kafle, A. Prabhakaran, O. Heber, M. Rappaport, H. Rubinstein, D. Schwalm, Y. Toker, and D. Zajfman, J. Phys. Chem. Lett. **5**, 4078 (2014).
[64] K. Peeters, E. Janssens, K. Hansen, P. Lievens, and P. Ferrari, Phys. Rev. Research **3**, 033225 (2021).
[65] R. Englman and J. Jortner, Mol. Phys. **18**, 145 (1970).
[66] E. S. Medvedev and V. I. Osherov, *Radiationless transitions in polyatomic molecules* (Springer-Verlag, 1995).
[67] D. J. Nesbitt and R. W. Field, J. Phys. Chem. **100**, 12735 (1996).
[68] M. Quack, Annu. Rev. Phys. Chem. **41**, 839 (1990).
[69] G. Mulas, Astron. Astrophys. **338**, 243 (1998).
[70] C. Lifshitz, Int. J. Mass Spectrom. **200**, 423 (2000).
[71] M. Basire, P. Parneix, T. Pino, P. Bréchignac, and F. Calvo, *PAHs and the Universe*, Vol. 46 (EDP Sciences, 2011) pp. 95–101.
[72] P. Parneix, M. Basire, and F. Calvo, J. Phys. Chem. A **117**, 3954 (2013).
[73] J. F. Durana and J. D. McDonald, J. Chem. Phys. **64**, 2518 (1976).
[74] D. J. Cook and R. J. Saykally, Astrophys. J. **493**, 793 (1998).

[75]C. Cohen-Tannoudji, B. Diu, and F. Laloë, *Quantum Mechanics*, Vol. 2 (Wiley-VCH, 2020).
[76]P. J. Robinson and K. A. Holbrook, *Unimolecular reactions* (Wiley-interscience, 1972).
[77]C. Lifshitz, Int. J. Mass Spectrom. **198**, 1 (2000).
[78]G. Sánchez, S. Díaz-Tendero, M. Alcamí, and F. Martín, Chem. Phys. Lett. **416**, 14 (2005).
[79]B. Concina, K. Głuch, S. Matt-Leubner, O. Echt, P. Scheier, and T. D. Märk, Chem. Phys. Lett. **407**, 464 (2005).
[80]K. Głuch, J. Fedor, S. Matt-Leubner, R. Parajuli, C. Mair, A. Stamatovic, O. Echt, C. Lifshitz, J. Harvey, F. Hagelberg, *et al.*, Eur. Phys. J. D **24**, 131 (2003).
[81]S. Tomita, J. U. Andersen, C. Gottrup, P. Hvelplund, and U. V. Pedersen, Phys. Rev. Lett. **87**, 073401 (2001).
[82]Y. F. Chang, J. P. Zhang, H. Sun, B. Hong, Z. An, and R. S. Wang, Int. J. Quantum Chem. **105**, 142 (2005).
[83]M. B. Sowa, P. A. Hintz, and S. L. Anderson, J. Chem. Phys. **95**, 4719 (1991).
[84]L. Montagnon and F. Spiegelman, Euro. Phys. J. D **43**, 7 (2007).
[85]K. Saha, V. Chandrasekaran, O. Heber, M. A. Iron, M. L. Rappaport, and D. Zajfman, Nature Comm. **9**, 912 (2018).
[86]F. Calvo, M. Basire, and P. Parneix, J. Phys. Chem. A **115**, 8845 (2011).
[87]K. A. Fichthorn and W. H. Weinberg, J. Chem. Phys. **95**, 1090 (1991).
[88]T. Beyer and D. F. Swinehart, Commun. ACM **16**, 379 (1973).
[89]J. R. Heath, R. F. Curl, and R. E. Smalley, J. Chem. Phys. **87**, 4236 (1987).
[90]J. Robertson and E. P. O'Reilly, Phys. Rev. B **35**, 2946 (1987).
[91]J. R. Platt, J. Chem. Phys. **17**, 484 (1949).
[92]I. Cherchneff and J. R. Barker, The Astrophysical Journal **341**, L21 (1989).
[93]R. M. Williams and S. R. Leone, The Astrophysical Journal **443**, 675 (1995).
[94]D. J. Cook, S. Schlemmer, N. Balucani, D. R. Wagner, B. Steiner, and R. J. Saykally, Nature **380**, 227 (1996).
[95]C. Falvo, H. Friha, T. Pino, Z. Dhaouadi, P. Parneix, F. Calvo, and P. Bréchignac, Phys. Chem. Chem. Phys. **15**, 10241 (2013).
[96]C. Falvo, F. Calvo, and P. Parneix, J. Chem. Phys. **137**, 064303 (2012).